The Astrophysical Journal Letters, 922:L6 (7pp), 2021 November 20 https://doi.org/10.3847/2041-8213/ac3664

Evidence for Mixing between ICM and Stripped ISM by the Analysis of the Gas Metallicity in the Tails of Jellyfish Galaxies

Andrea Franchetto[1,2], Stephanie Tonnesen[3], Bianca M. Poggianti[2], Benedetta Vulcani[2], Marco Gullieuszik[2], Alessia Moretti[2], Rory Smith[4], Alessandro Ignesti[2], Cecilia Bacchini[2], Sean McGee[5], Neven Tomičić[2], Matilde Mingozzi[6], Anna Wolter[7], and Ancla Müller[8]
[1] Dipartimento di Fisica e Astronomia "Galileo Galilei," Università di Padova, vicolo dell'Osservatorio 3, I-35122 Padova, Italy; andrea.franchetto@phd.unipd.it
[2] INAF—Astronomical Observatory of Padova, vicolo dell'Osservatorio 5, I-35122 Padova, Italy
[3] Flatiron Institute, CCA, 162 5th Avenue, New York, NY 10010, USA
[4] Korea Astronomy and Space Science Institute (KASI), 776 Daedeokdae-ro, Yuseong-gu, Daejeon 34055, Republic of Korea
[5] School of Physics and Astronomy, University of Birmingham, Birmingham B15 2TT, UK
[6] Space Telescope Science Institute, 3700 San Martin Drive, Baltimore, MD 21218, USA
[7] INAF—Osservatorio Astronomico di Brera, via Brera 28, I-20121 Milano, Italy
[8] Ruhr University Bochum, Faculty of Physics and Astronomy, Astronomical Institute, Universitätsstr. 150, 44801 Bochum, Germany
Received 2021 September 24; revised 2021 October 27; accepted 2021 November 3; published 2021 November 17

Abstract

Hydrodynamical simulations show that the ram pressure stripping in galaxy clusters fosters a strong interaction between stripped interstellar medium (ISM) and the surrounding medium, with the possibility of intracluster medium (ICM) cooling into cold gas clouds. Exploiting the MUSE observation of three jellyfish galaxies from the GAs Stripping Phenomena in galaxies with MUSE (GASP) survey, we explore the gas metallicity of star-forming clumps in their gas tails. We find that the oxygen abundance of the stripped gas decreases as a function of the distance from the parent galaxy disk; the observed metallicity profiles indicate that more than 40% of the most metal-poor stripped clouds are constituted by cooled ICM, in qualitative agreement with simulations that predict mixing between the metal-rich ISM and the metal-poor ICM.

Unified Astronomy Thesaurus concepts: Galaxy clusters (584); Intracluster medium (858); Ram pressure stripped tails (2126); Interstellar abundances (832)

1. Introduction

Cluster galaxies that move with high velocities (∼1000 $\mathrm{km\,s^{-1}}$) through the hot and dense intracluster medium (ICM; $T \sim 10^7$–10^8 K, $n_e \sim 10^{-4}$–$10^{-2}\,\mathrm{cm^{-3}}$; Sarazin 1986) can be affected by ram pressure stripping (RPS; Gunn & Gott 1972) that is able to eradicate their interstellar medium (ISM).

The interaction between the ISM and the ICM can be extremely complex, and hydrodynamical simulations, which study the mixing process between the two fluids, consider several processes: cloud destruction via Kelvin–Helmholtz instabilities (Chandrasekhar 1961) and the heating of the stripped ISM with subsequent evaporation into the ICM (Cowie & McKee 1977), as well as the radiative cooling of the ICM onto cold gas clouds (Klein et al. 1994; Gronke & Oh 2018). Tonnesen & Bryan (2021) find that the latter mixing scenario is possible in a high-density and low-velocity ICM wind, providing a guide for observational studies.

Observationally, the stripped gas has a multiphase nature: H I (e.g., Chung et al. 2009), molecular gas (e.g., Jáchym et al. 2017), Hα (e.g., Gavazzi et al. 2001), and X-ray gas (e.g., Sun et al. 2010). In particular, the ionized gas-phase is often due to the photoionization by radiation coming from young stars formed in situ (Poggianti et al. 2019a). The optical emission lines of this ionized medium allow us to study several properties of the gas, like the gas-phase metallicity. This quantity can be an excellent tracer to evaluate the mixing scenario between the metal-rich ISM (Maiolino & Mannucci 2019) and the metal-poor ICM (Mernier et al. 2018), bridging the gap between simulations and observations. Recently, the galaxies with the GAs Stripping Phenomena in galaxies with MUSE (GASP) project (Poggianti et al. 2017) have provided a statistically significant sample of RPS galaxies, probing various gas properties (e.g., star formation rate, ionization mechanisms, kinematics) both in the galaxy disk and in the stripped tails (Gullieuszik et al. 2017; Poggianti et al. 2019a; Vulcani et al. 2020). However, neither any of the GASP papers (Gullieuszik et al. 2017; Poggianti et al. 2017; Bellhouse et al. 2019) nor other studies (Yoshida et al. 2012; Fossati et al. 2016; Merluzzi et al. 2016; Consolandi et al. 2017) focused solely on the gas metallicity in the tails of jellyfish galaxies.[9]

In this Letter we exploit the MUSE observations of the GASP survey to track the gas-phase metallicity along the tails of the most striking jellyfish galaxies to investigate the interaction between the ISM and ICM during RPS. Our analysis provides for the first time key constraints to theoretical models investigating the mixing between the two media.

2. Galaxy Sample

To suitably investigate the metallicity profiles in the tails of RPS galaxies, we select from the GASP sample the cluster galaxies with the longest tails and tentacles of ionized gas—traced by the Hα emission—unilaterally displayed with respect to the main galaxy body. Four galaxies with stripped ionized

[9] The term "jellyfish galaxies" generally indicates RPS galaxies with spectacular, long gas tails.

Table 1
Properties of the Analyzed Galaxies

ID (1)	R.A. (J2000) (2)	Decl. (J2000) (3)	z (4)	$\log(M_\star/M_\odot)$ (5)	$12+\log(\mathrm{O/H})_{Re}$ (6)	$\alpha_{\mathrm{O/H}}$ (dex/R_e) (7)	Main Reference (8)
JO206	21:13:47.41	+02:28:34.383	0.0489	$10.96^{+0.04}_{-0.05}$	8.96 ± 0.07	-0.10 ± 0.02	Poggianti et al. (2017)
JW100	23:36:25.06	+21:09:02.529	0.0551	$11.5^{+0.1}_{-0.1}$	9.24 ± 0.01	-0.04 ± 0.01	Poggianti et al. (2019b)
JW39	13:04:07.71	+19:12:38.486	0.0634	$11.21^{+0.07}_{-0.08}$	9.12 ± 0.06	-0.04 ± 0.01	Poggianti et al. (2019a)

Note. Columns are (1) GASP ID number; (2) and (3) equatorial coordinates of the galaxy center; (4) redshift; (5) logarithm of the stellar mass taken from Vulcani et al. (2018); (6) gas metallicity at the effective radius from Franchetto et al. (2020); (7) metallicity radial gradient from Franchetto et al. (2021); (8) main references. Further information and images are published in Gullieuszik et al. (2020) and on the GASP website https://web.oapd.inaf.it/gasp/.

gas reaching over 50 kpc (in projection) from the galaxy center, represent the best candidates for this study: JO201, JO206, JW100, and JW39.

Since the metallicity profile of the ram pressure stripped gas from JO201 is already published in Bellhouse et al. (2019), in this Letter we mainly present the results based on the other three galaxies, discussing the implications for JO201 only in the text. The properties of the analyzed galaxies are presented in Table 1.

3. Data Analysis

As extensively explained in Poggianti et al. (2017): MUSE spectra are corrected for the extinction due to our Galaxy. The stellar-only component is derived applying our spectrophotometric fitting code SINOPSIS (Fritz et al. 2017) and then subtracted from each spectrum. The gas kinematics, emission line fluxes, and corresponding errors are derived using the software KUBEVIZ that fits Gaussian line profiles (Fossati et al. 2016). Then, the fluxes are corrected for the internal dust extinction assuming a Balmer decrement of $\mathrm{H}\alpha/\ \mathrm{H}\ \beta = 2.86$ and applying the extinction law of Cardelli et al. (1989).

We adopt the BPT diagnostic diagrams (Baldwin et al. 1981) based on the [N II]λ6583 and [S II]$\lambda\lambda$6717, 31 emission lines to select only star-forming regions whose line ratios are below the separation curves of both Kewley et al. (2001) and Kewley et al. (2006). This cross-check more accurately excludes regions powered by ionizing sources different from star formation.

The metallicity of the ionized gas is estimated making use of a modified version of the code PYQZ (Dopita et al. 2013; Vogt et al. 2015; F. Vogt 2017, private communication). PYQZ interpolates the observed line ratios [N II]λ6583/[S II]$\lambda\lambda$6717, 31 and [O III]λ5007/[S II]$\lambda\lambda$6717, 31 on a model grid computed by MAPPINGS IV, able to disentangle degeneracy with the ionization parameter (Sutherland & Dopita 1993; Dopita et al. 2013), and delivers the oxygen abundance $12+\log(\mathrm{O/H})$ that here we use as a tracer of the gas-phase metallicity, and the associated error by the propagation of the flux uncertainties.

Disks and tails of jellyfish galaxies are characterized by bright Hα clumps, identified to be star-forming clumps surrounded by regions of more diffuse emission (Poggianti et al. 2019a). These clumps are defined as circular regions centered to the local minima of the Laplace+median filtered Hα-MUSE image. The radius of clumps is determined by a recursive algorithm that evaluates the inner counts above the surrounding diffuse emission (see Poggianti et al. 2017 for details). Spectra within each clump are added, and integrated properties are derived as explained before. Clump integrated spectra reach a high signal-to-noise ratio (S/N; $(\mathrm{S/N})_{\mathrm{H}\alpha} \sim 90$, on average); therefore, in the following, we focus on these regions. These clumps are sufficiently massive ($> 10^5\,M_\odot$; Poggianti et al. 2019a) to exclude effects due to incomplete initial mass function (IMF) sampling.

The gas-phase metallicity maps of the ionized gas and the identified clumps for JW100, JO206, and JW39 are presented in Figures 1(a), 2(a), and 3(a), respectively. The dashed contours in the figures indicate the galaxy body, defined as the stellar continuum flux 1σ above the background level (Poggianti et al. 2017).

3.1. Tails and Subtails

The goal of this work is to explore the distribution of the gas metallicity along the jellyfish galaxy tails. However, the ISM is removed from different positions of the galaxy disk, and the orientation of the stripped gas in the three-dimensional space is unknown. Therefore, to perform an analysis as accurate as possible, for each galaxy, we identify several main subtails, selecting those clumps that are aligned along gas tentacles and, according to the gas kinematics, have similar line-of-sight velocities. Indeed, observations and simulations show that, in most cases, the stripped gas maintains the rotation it had in the disk (Merluzzi et al. 2013; Gullieuszik et al. 2017). When it is feasible, we also include a maximum of three clumps in the galaxy body to statistically determine the metallicity value of the disk gas in the point where the tail stems from. Since projection effects prevent a clear distinction, such a value is a lower limit because the gas of those clumps might be already stripped.

In Figures 1(b), 2(b), and 3(b), we show for each galaxy the clumps belonging to different subtails, according to our selection. Focusing separately on each subtail allows us to better highlight gas-metallicity trends with the projected distance, minimizing the scatter due to the uncertainties on the spatial projection.[10]

To suitably estimate the projected distance of the stripped clumps from the galaxy, we measure their position parallel to the specific stripping direction of the corresponding subtail. This direction is calculated by a linear fit of the clumps of each given subtail, and is indicated by an arrow in panel (b) of the figures. Distances are converted in kpc according to the redshift of the host cluster and then normalized, imposing that the zero-point coincides with the first clump in the subtail (including those in the galaxy body). In this sense, these distances have to be interpreted as reference positions measured along the subtail, and these values are lower limits of the real distances anyway, as they are estimated on the sky plane.

[10] We note that the northern subtail of JO206 might be quite uncertain, but removing it from the analysis does not impact the results.

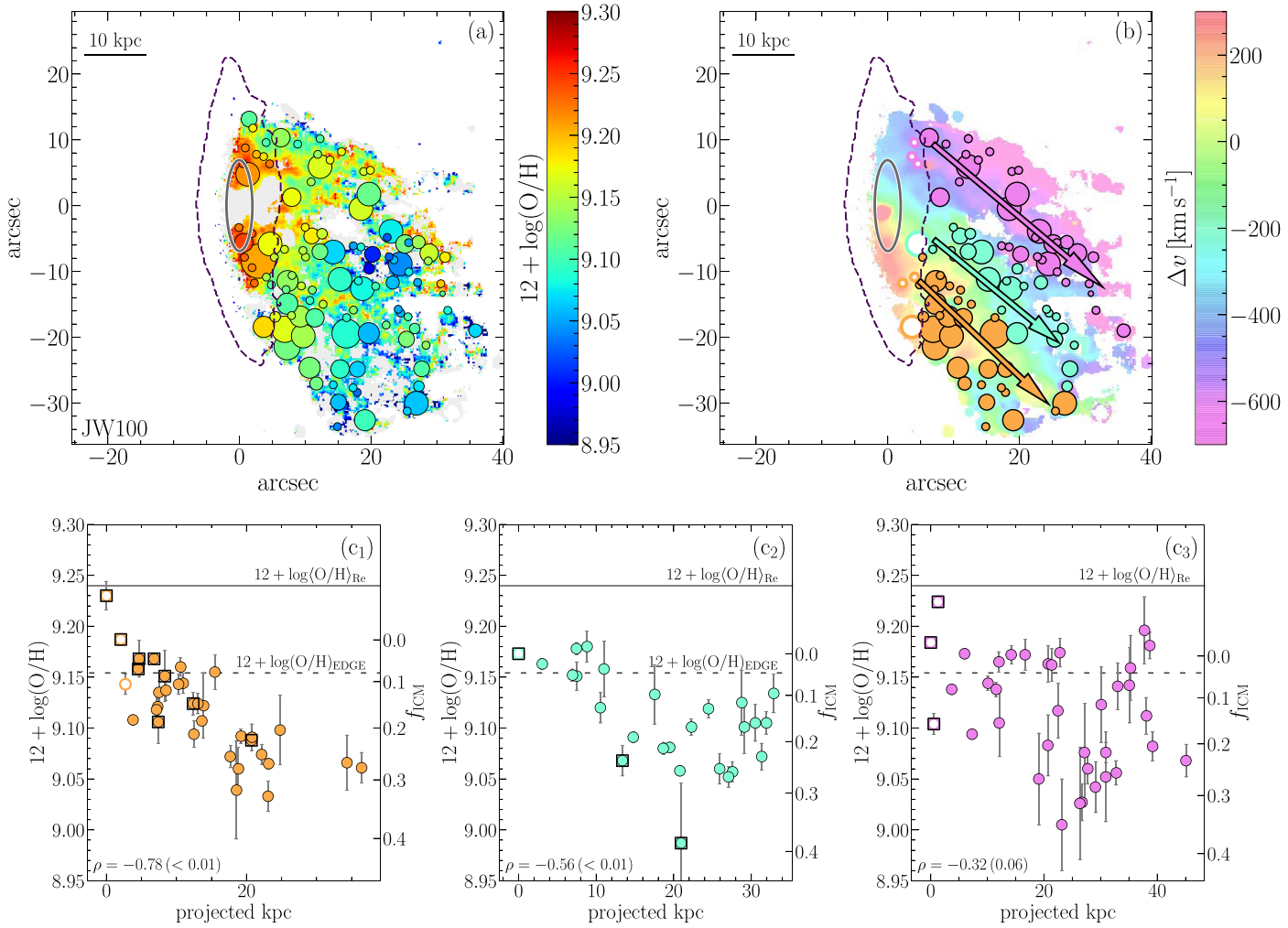

Figure 1. JW100. Panel (a): gas-phase metallicity map. The circles identify the position and the size of the star-forming clumps. Underlying gray spaxels correspond to the distribution of the Hα emission with a signal-to-noise ratio greater than 5. Panel (b): color-coded gas velocity field map with superimposed clumps belonging to different subtails. Each subtail is identified by a different color (not correlated to the color bar). Open dots correspond to clumps inside the galaxy body. The arrows indicate the direction of the stripping for each subtail. In panels (a) and (b), the dashed contour shows the galaxy body and the gray ellipse indicates the effective radius. Panels (c1)–(c3): projected metallicity profile of each subtail. Dots and error bars refer to clump metallicities and associated uncertainties, respectively. Square frames indicate star-forming clumps according to [O I]-BPT. Colors correspond to panel (b). Gray horizontal lines and the faded areas denote the metallicity at the effective radius and the corresponding uncertainty. Dashed lines indicate the expected metallicity at the edge of the stellar body. In the bottom left corner we also report the Pearson correlation coefficient (and the corresponding p-value) of the observed trends. The scale on the right y-axis indicates the fraction of ICM as explained in the text.

We highlight that the results are independent on the choice of the zero-point, and in addition, the metallicity trends persist also when the tail is explored as a whole, but at the expense of an increased scatter.

4. Results

Figures 1(a), 2(a), and 3(a) clearly show that the gas metallicities in the tails of all galaxies are systematically lower than those in the galaxy disks. These trends are better identified looking at Figures 1(c1)–(c3), 2(c1)–(c4), and 3(c1)–(c2), where we present the distribution of the metallicities of the clumps in each selected subtail against their position along the tail. As a reference of the metallicity in the disk, for each galaxy we indicate (with a horizontal solid line) the value at the effective radius taken from Franchetto et al. (2020). In most cases, metallicities in the tails are much lower than this value. Furthermore, in all subtails we detect a decrease of the gas metallicity moving along the stripping direction; the decrease varies between $\sim$0.1 and $\sim$0.4 dex, with the lowest metallicities mainly located in the furthest regions. A similar behavior is also observed in JO201, whose tail metallicity trends are very similar to those of the three galaxies presented here; as shown in Figure 6 of Bellhouse et al. (2019), the metallicities of clumps in the tail decrease by $\sim$0.5 dex moving away from the galaxy center, along 60 projected kpc of distance. For each subtail, we also compute the Pearson correlation coefficient ρ (along with the corresponding p-value) to attest to the relevance of these gas-metallicity trends; we find a strong decreasing relationship ($|\rho| > 0.5$) in most subtails with a high statistical significance (p-value $\leqslant 0.07$).

5. Discussion and Summary

In previous works, the observed decreasing metallicity profiles along the stripped gas tails have been interpreted as a consequence of the RPS mechanism, which first removes the outermost, metal-poor gas and subsequently the higher-

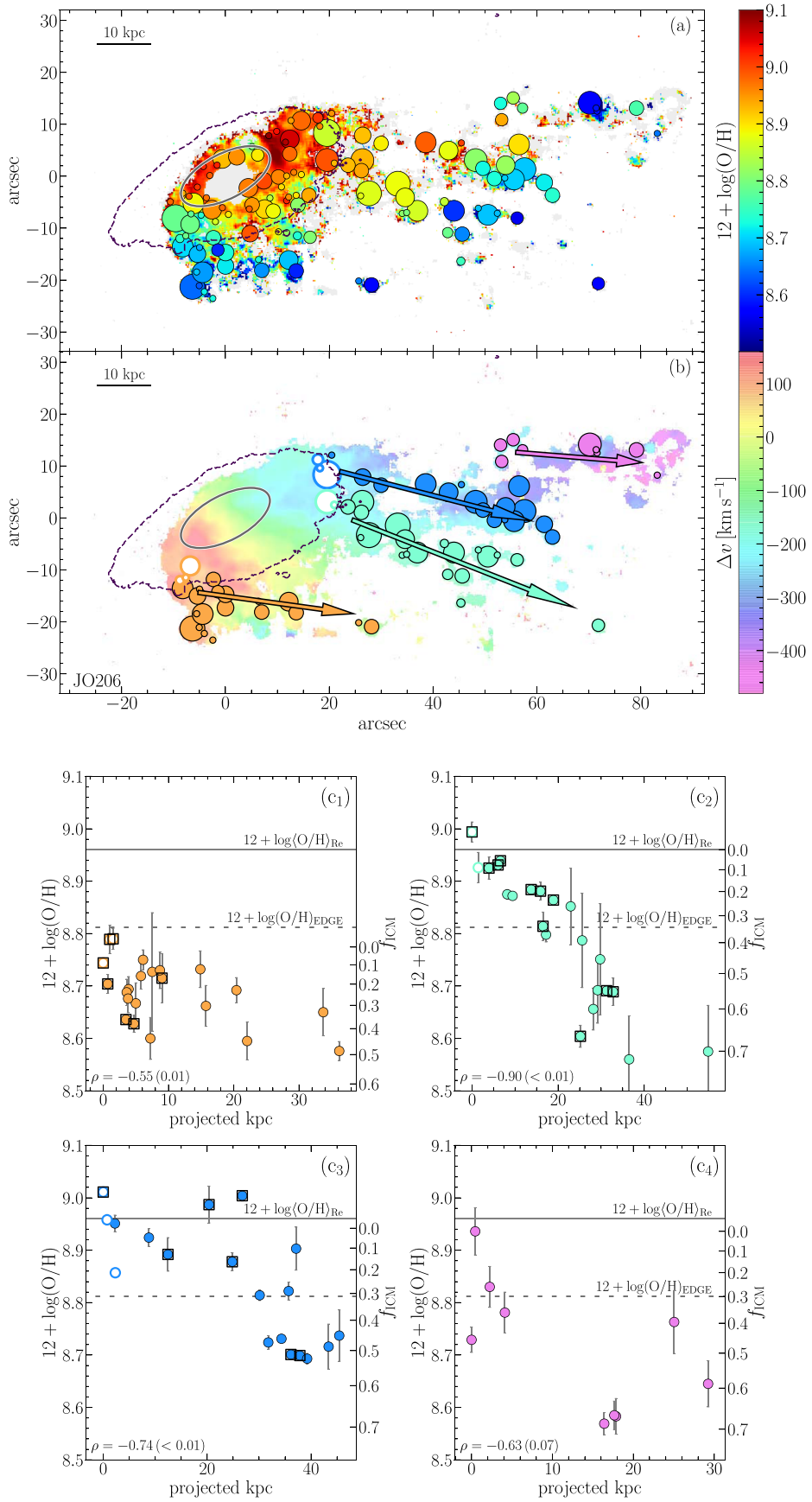

Figure 2. JO206. The panels are as in Figure 1.

metallicity gas closer to the galaxy center, following the

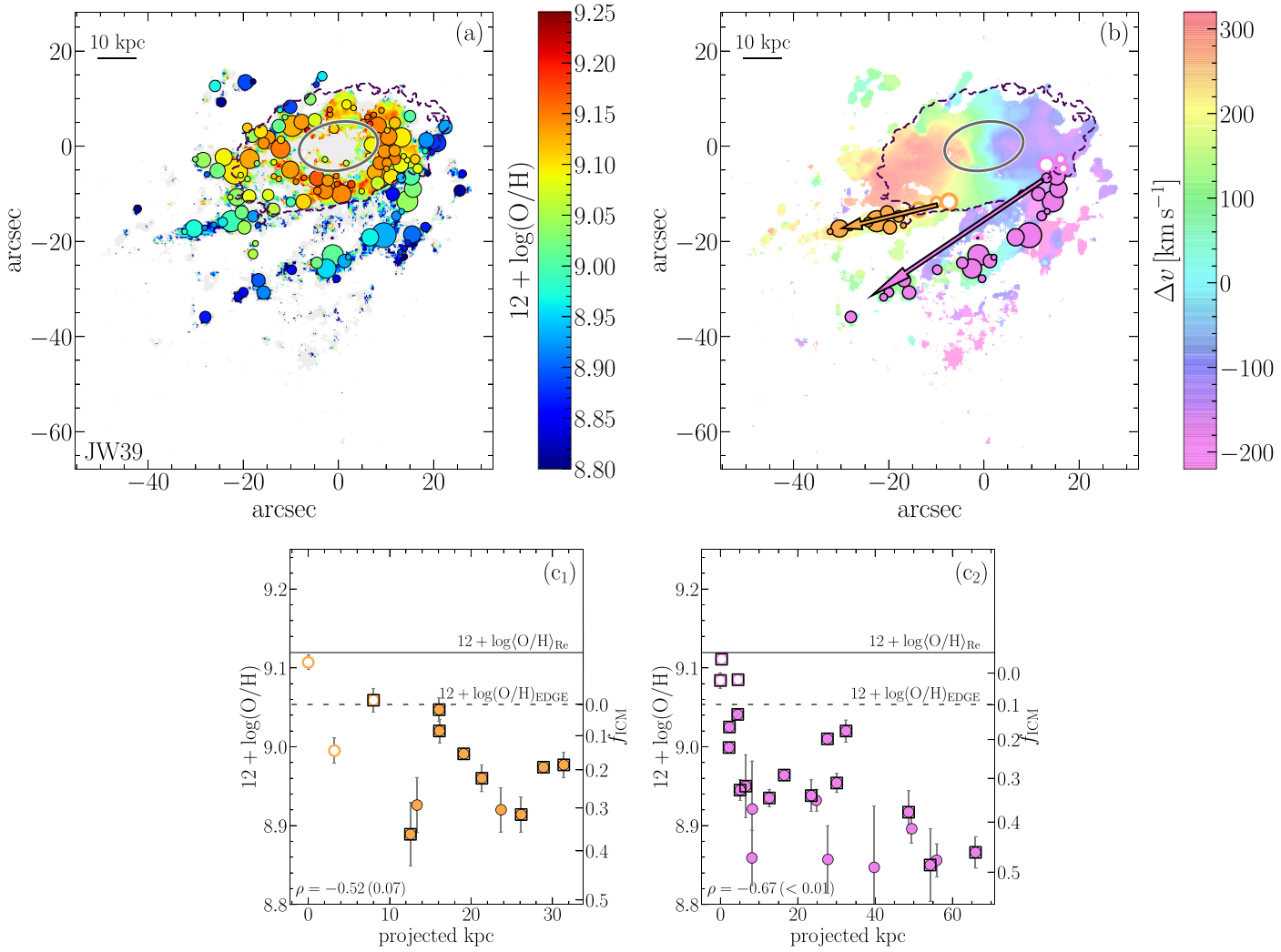

Figure 3. JW39. The panels are as in Figure 1.

metallicity radial profile of galaxies (Gullieuszik et al. 2017; Poggianti et al. 2017; Bellhouse et al. 2019). Here, we argue that this effect, although plausible, is not sufficient to explain the trends in the analyzed jellyfish galaxies. Indeed, massive galaxies ($M_\star \geqslant 10^{11}\,M_\odot$), such as those presented here, have, on average, high gas-metallicity values and very shallow metallicity profiles, shallower than intermediate-mass galaxies (Sánchez-Menguiano et al. 2016; Franchetto et al. 2021). In particular, according to the gas-metallicity gradients estimated in the galaxy body of these three galaxies (Franchetto et al. 2021), the metallicity values at the edge of the stellar disk (indicated with a dashed line in Figures 1(c1)–(c3), 2(c1)–(c4), and 3(c1)–(c2)) are still much higher than those reached in tails.

Therefore, we consider three possible scenarios to explain the observed trends and the low metallicity values in the tails: (1) the progressively lower-metallicity gas that is observed farther out in the tail might have been removed from the gas disk at large galactocentric radii, beyond the stellar galaxy body, where metallicities are expected to be lower than within the stellar disk; (2) the particular physical conditions of the gas are leading to an erroneous metallicity estimation; and (3) the metallicity values in the tails are due to mixing with the metal-poor ICM. The additional hypothesis that lower-density gas, which is more easily stripped, has lower metallicities is ruled out by our previously published results, showing that gas clumps and diffuse gas have on average similar metallicities (Tomicic et al. 2021).

Scenario (1) would require the tail to narrow with distance and that the gas stripped outside migrates to smaller radii (where the radius is defined as the radius of the approximately cylindrical section of the tail identified by a plane parallel to the galaxy disk at any given distance). In particular, assuming the metallicity gradients estimated in the disk of these galaxies (Franchetto et al. 2021) and hypothesizing that they extend over the stellar body without flattening, the most metal-poor clump gas detected in the tails should have been stripped approximately from galactic radii twice as large as the stellar disk radius. This is unrealistic for two reasons: simulations show that the tails maintain their radius or, if anything, get wider with distance from the disk (Tonnesen & Bryan 2010, 2021); both observations and simulations agree that stripped gas maintains its orbital velocity (Merluzzi et al. 2013; Gullieuszik et al. 2017; see also the top right panels of our figures), and therefore it is not falling to smaller radial distances.

Moreover, looking at our observed tails in their entirety, their radius approximately coincides with the extent of the stellar

disk, and all but one of our subtails are anchored in the disk. This indicates that the observed ionized gas was not stripped from well beyond the stellar disk.

Scenario (2) considers the possibility that contamination of an additional ionization source might alter the observed line ratios. This would yield incorrect metallicity estimates along the tail because the model grids adopted by PYQZ are designed including only photoionization from young massive stars. Evidence for additional ionization mechanisms in some tails, likely due to the interaction of ICM–ISM, is based on an excess of the [O I]λ6300 line (Poggianti et al. 2019a; Campitiello et al. 2021; Tomicic et al. 2021). Although this effect is seen in particular in the diffuse gas (outside of clumps) and we paid particular attention to select only star-forming clumps, we perform a further check excluding those clumps that are not powered by star formation according to the BPT diagram based on the [O I] line, adopting the separation curve of Kewley et al. (2006). Although this selection preserves only a third of the valid clumps (square-framed dots in the bottom panels of Figures 1, 2, and 3), in all three galaxies we still find a clear metallicity profile along the tails. As an additional check, we also reanalyze the profiles computing the metallicities with the O3N2 calibration of Curti et al. (2017) (plots not shown) finding that the correlation still holds. This confirms that the observed trends are real and not due to a systematic bias in the metallicity estimates. However, in principle, we cannot rule out the effect of exotic processes that might produce artifacts in the metallicity measurement, but we are not in a position to evaluate it.

Scenario (3) invokes the mixing between the stripped ISM and the ICM, observed in some simulation works (e.g., Gronke & Oh 2018; Tonnesen & Bryan 2021). X-ray observations find that clusters are characterized by a uniform iron abundance of $Z_{\rm Fe} \sim 0.3$ solar beyond a 0.2–0.3 virial radius (Mernier et al. 2018). As our galaxies present supersolar metallicities in their disks, a mixture of these two components could produce an evident decrease of metallicity proportional to the amount of ICM cooled in the stripped material. A rough estimate of the ICM fraction in the clumps can be done assuming that the observed metallicity in tails is a linear combination of the stripped ISM and ICM metallicities weighted by the fraction of the two components:

$$Z_{\rm obs} = Z_{\rm ISM} f_{\rm ISM} + Z_{\rm ICM} f_{\rm ICM}, \quad (1)$$

where the metallicities are expressed in solar units[11] and $f_{\rm ISM} + f_{\rm ICM} = 1$.

Unfortunately, $Z_{\rm ISM}$ and $Z_{\rm ICM}$ are not well constrained; therefore, we need to make some assumptions, trying to be as conservative as possible. In the absence of an accurate measure of the ICM metallicity around our galaxies, we set $Z_{\rm ICM} = 0.3$. The $Z_{\rm ISM}$ of each subtail is the mean metallicity of corresponding clumps inside the disk, or in the absence of them the highest value observed among the selected clumps. By this simple calculation, we can obtain the $f_{\rm ICM}$ values corresponding to metallicities detected in each subtail. These values are reported on the right y-axis of Figures 1(c1)–(c3), 2(c1)–(c4), and 3(c1)–(c2). For JW100 and JW39 we derive that ∼30%–40% of the most metal-poor clumps could be constituted by gas from the ICM, for JO206 the mixing can reach values as high as ∼60%, while for JO201 the effect is evaluated up to the 80%.

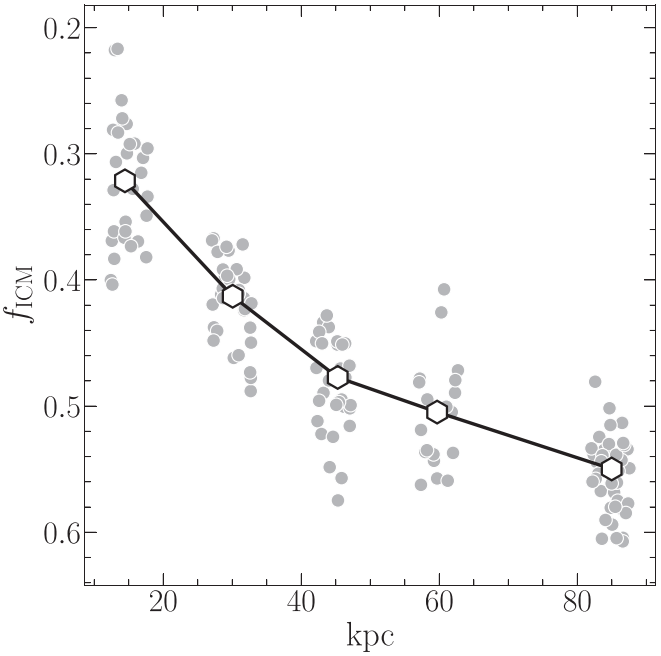

Figure 4. The distribution of $f_{\rm ICM}$ in clumps identified in a snapshot of the tail of a simulated RPS galaxy (440 Myr in HDLV from Tonnesen & Bryan 2021) as a function of the distance from the galaxy. Gray dots refer to the values of clumps, while white hexagons indicate the median value at each given distance.

We stress that these values are only indicative as they can suffer from large uncertainties due to the simplistic estimation. Despite these qualifications, we can make a qualitative comparison with the simulated RPS galaxies presented in Tonnesen & Bryan (2021), who study the mixing of the galactic gas with the ICM wind. In detail, we select similar regions from the tail of one of their three RPS galaxies (HDLV from that work). We use the clump finder routine in YT (Turk et al. 2011) to find groups of at least 200 connected cells above the threshold density of 10^{-26} g cm^{-3}, for which we compute their mass-weighted positions; to mimic the MUSE observations, we select spherical 1 kpc regions centered on these positions with at least 20 dense cells ($\rho > 10^{-24}$ g cm^{-3}); these dense cells are used to derive the mass-weighted ICM fraction of each of these clumps and their distance from the galaxy disk.

In Figure 4, we find a clear trend between the $f_{\rm ICM}$ in clumps and their physical distance from the simulated galaxy: moving from 15 kpc to 85 kpc, the amount of ICM cooled in the clumps increases from 32% to 55%, on average, of the total clump mass, with fluctuations inside a spread of 10%. While the exact values vary, the trend holds in all three Tonnesen & Bryan (2021) simulations across hundreds of Myr, and is discussed in detail in Tonnesen & Bryan (2021). Although a direct quantitative comparison is not possible due to the differences in the ICM properties, galaxy masses, and orbits, as well as projection effects, simulations agree with our observations and support the ISM–ICM mixing scenario.

Finally, since we are focusing on gas of clumps involved in recent star formation, we should expect a metal enrichment due to the stellar yields, conversely to observations. Therefore, finding low metallicities contributes to reinforcing the hypothesis of mixing.

[11] $\log(Z[Z_\odot]) = 12 + \log({\rm O/H}) - 8.69$, where 8.69 is the solar oxygen abundance adopted by PYQZ.

To summarize, in this Letter we showed three cases of ram pressure stripped galaxies where star-forming clumps in the tails have lower metallicity at larger galactic distances. The metallicity decrease is much larger than the expected trend due to the outside-in stripping, and we argue that ISM–ICM mixing is needed, in good agreement with predictions from simulations. Thus, a picture in which clouds are stripped intact directly from the disk and survive unmixed is inconsistent with the observations shown here. Even dense gas clumps seem to be well mixed with the ICM.

We thank the GASP team for useful discussions. Based on observations collected at the European Organization for Astronomical Research in the Southern Hemisphere under ESO program 196.B-0578. This project has received funding from the European Research Council (ERC) under the European Union's Horizon 2020 research and innovation program (grant agreement No. 833824, PI: Poggianti). We acknowledge funding from the INAF main-stream funding program (PI: B. Vulcani). B.V. and M.G. acknowledge the Italian PRIN-Miur 2017 (PI: A. Cimatti). S.M. acknowledges support from the Science and Technology Facilities Council through grant No. ST/N021702/1.

Software: SINOPSIS (Fritz et al. 2017), KUBEVIZ (Fossati et al. 2016), PYQZ (Dopita et al. 2013; Vogt et al. 2015), YT (Turk et al. 2011).

ORCID iDs

Andrea Franchetto https://orcid.org/0000-0001-9575-331X
Stephanie Tonnesen https://orcid.org/0000-0002-8710-9206
Bianca M. Poggianti https://orcid.org/0000-0001-8751-8360
Benedetta Vulcani https://orcid.org/0000-0003-0980-1499
Marco Gullieuszik https://orcid.org/0000-0002-7296-9780
Alessia Moretti https://orcid.org/0000-0002-1688-482X
Rory Smith https://orcid.org/0000-0001-5303-6830
Alessandro Ignesti https://orcid.org/0000-0003-1581-0092
Cecilia Bacchini https://orcid.org/0000-0002-8372-3428
Sean McGee https://orcid.org/0000-0003-3255-3139
Neven Tomičić https://orcid.org/0000-0002-8238-9210
Matilde Mingozzi https://orcid.org/0000-0003-2589-762X
Anna Wolter https://orcid.org/0000-0001-5840-9835
Ancla Müller https://orcid.org/0000-0001-9184-7845

References

Baldwin, J. A., Phillips, M. M., & Terlevich, R. 1981, PASP, 93, 5
Bellhouse, C., Jaffé, Y. L., McGee, S. L., et al. 2019, MNRAS, 485, 1157
Campitiello, M. G., Ignesti, A., Gitti, M., et al. 2021, ApJ, 911, 144
Cardelli, J. A., Clayton, G. C., & Mathis, J. S. 1989, ApJ, 345, 245
Chandrasekhar, S. 1961, Hydrodynamic and Hydromagnetic Stability (Oxford: Clarendon)
Chung, A., van Gorkom, J. H., Kenney, J. D. P., Crowl, H., & Vollmer, B. 2009, AJ, 138, 1741
Consolandi, G., Gavazzi, G., Fossati, M., et al. 2017, A&A, 606, A83
Cowie, L. L., & McKee, C. F. 1977, ApJ, 211, 135
Curti, M., Cresci, G., Mannucci, F., et al. 2017, MNRAS, 465, 1384
Dopita, M. A., Sutherland, R. S., Nicholls, D. C., Kewley, L. J., & Vogt, F. P. A. 2013, ApJS, 208, 10
Fossati, M., Fumagalli, M., Boselli, A., et al. 2016, MNRAS, 455, 2028
Franchetto, A., Mingozzi, M., Poggianti, B. M., et al. 2021, arXiv:2109.02656
Franchetto, A., Vulcani, B., Poggianti, B. M., et al. 2020, ApJ, 895, 106
Fritz, J., Moretti, A., Gullieuszik, M., et al. 2017, ApJ, 848, 132
Gavazzi, G., Boselli, A., Mayer, L., et al. 2001, ApJL, 563, L23
Gronke, M., & Oh, S. P. 2018, MNRAS, 480, L111
Gullieuszik, M., Poggianti, B. M., McGee, S. L., et al. 2020, ApJ, 899, 13
Gullieuszik, M., Poggianti, B. M., Moretti, A., et al. 2017, ApJ, 846, 27
Gunn, J. E., Gott, J., & Richard, I. 1972, ApJ, 176, 1
Jáchym, P., Sun, M., Kenney, J. D. P., et al. 2017, ApJ, 839, 114
Kewley, L. J., Dopita, M. A., Sutherland, R. S., Heisler, C. A., & Trevena, J. 2001, ApJ, 556, 121
Kewley, L. J., Groves, B., Kauffmann, G., & Heckman, T. 2006, MNRAS, 372, 961
Klein, R. I., McKee, C. F., & Colella, P. 1994, ApJ, 420, 213
Maiolino, R., & Mannucci, F. 2019, A&ARv, 27, 3
Merluzzi, P., Busarello, G., Dopita, M. A., et al. 2013, MNRAS, 429, 1747
Merluzzi, P., Busarello, G., Dopita, M. A., et al. 2016, MNRAS, 460, 3345
Mernier, F., Biffi, V., Yamaguchi, H., et al. 2018, SSRv, 214, 129
Poggianti, B. M., Gullieuszik, M., Tonnesen, S., et al. 2019a, MNRAS, 482, 4466
Poggianti, B. M., Ignesti, A., Gitti, M., et al. 2019b, ApJ, 887, 155
Poggianti, B. M., Moretti, A., Gullieuszik, M., et al. 2017, ApJ, 844, 48
Sánchez-Menguiano, L., Sánchez, S. F., Pérez, I., et al. 2016, A&A, 587, A70
Sarazin, C. L. 1986, RvMP, 58, 1
Sun, M., Donahue, M., Roediger, E., et al. 2010, ApJ, 708, 946
Sutherland, R. S., & Dopita, M. A. 1993, ApJS, 88, 253
Tomicic, N., Vulcani, B., Poggianti, B. M., et al. 2021, arXiv:2108.12433
Tonnesen, S., & Bryan, G. L. 2010, ApJ, 709, 1203
Tonnesen, S., & Bryan, G. L. 2021, ApJ, 911, 68
Turk, M. J., Smith, B. D., Oishi, J. S., et al. 2011, ApJS, 192, 9
Vogt, F. P. A., Dopita, M. A., Borthakur, S., et al. 2015, MNRAS, 450, 2593
Vulcani, B., Poggianti, B. M., Gullieuszik, M., et al. 2018, ApJL, 866, L25
Vulcani, B., Poggianti, B. M., Tonnesen, S., et al. 2020, ApJ, 899, 98
Yoshida, M., Yagi, M., Komiyama, Y., et al. 2012, ApJ, 749, 43